J. Fluid Mech. (1983), *vol.* 132, *pp.* 349–373
Printed in Great Britain

Tests of subgrid models in the near-wall region using represented velocity fields

By Y. KANEDA† AND D. C. LESLIE
Department of Nuclear Engineering, Queen Mary College, Mile End Road, London E1 4NS

(Received 27 October 1982 and in revised form 16 March 1983)

The 2.5-dimensional model of the turbulent field near a wall, proposed by Hatziavramidis & Hanratty (1979) and modified by Chapman & Kuhn (1981), has been used to test the subgrid models of Schumann (1973, 1975) and Moin & Kim (1982). The results are disquieting, both trends and orders of magnitude sometimes being seriously in error. It also appears that the contribution of the subgrid energy to the pseudopressure calculated in large-eddy simulations can be large, although this contribution is usually neglected. On the positive side, Leonard's model for the Leonard stress is extremely good, and Schumann's synthetic boundary condition is also found to be reliable.

These results must be taken with a grain of salt, since the tests reported in §5 show that the 2.5-dimensional model cannot reproduce important characteristics of the turbulence in the neighbourhood of $y^+ = 40$.

1. Introduction

Many attempts have been made to represent the turbulent velocity field in the neighbourhood of a solid wall using simplified analytical or numerical procedures. The paper of Schubert & Corcos (1967) is typical of earlier attempts, which, though interesting, produced fields which did not agree at all closely with experiment.

A substantial step forward was taken by Hatziavramidis & Hanratty (1979), who combined an outer boundary condition representative of the spanwise streaks with the assumption that the streamwise derivatives are negligibly small. This assumption, which is inferred from the experimental observation that the streaks are much extended in the streamwise direction, reduces the dimensionality of the problem and makes it possible to generate sample velocity fields without excessive computation. The fields generated in this way are periodic rather than random (because the outer boundary condition is periodic) but, as Hatziavramidis & Hanratty showed, this is no obstacle to using them as representations of true turbulence.

Chapman & Kuhn (1981) have improved the outer boundary condition by careful analysis of the experimental data, and we have used both types of boundary condition.

Our objective has been to test the subgrid models proposed by Schumann (1973, 1975) and by Moin & Kim (1982) for use in large-eddy simulations of turbulent flows in channels and other simple geometries. Since we have a detailed representation of the field, we can compute the 'actual' subgrid stresses and compare these 'actual' values with those generated by the models.

† Permanent address: Department of Applied Physics, Nagoya University, Nagoya, Japan.

This approach to the testing of subgrid models was pioneered for homogeneous fields by Clark, Ferziger & Reynolds (1979). They were able to do a full simulation on a fine mesh (64^3) and then to test the models on coarser meshes. Wehave not been able to do this, since a full simulation of a turbulent channel flow is quite out of reach at present, even for low Reynolds numbers. We have therefore had to use the 2.5-dimensional representation of Hatziavramidis & Hanratty and of Chapman & Kuhn, and our work cannot have the authority and accuracy of that of Clark *et al.*

We have not found it easy to reproduce the results of Hatziavramidis & Hanratty and of Chapman & Kuhn, and the paper begins with an account of the problems we have encountered. We have also used the represented fields to examine the behaviour of k and ϵ near the wall.

2. 2.5-dimensional model simulation of viscous-sublayer turbulence

Under the assumption that the velocity derivatives in the streamwise (x) direction are negligible, the Navier–Stokes and continuity equations for an incompressible fluid simplify to

$$\frac{\partial u}{\partial t}+v\frac{\partial u}{\partial y}+w\frac{\partial u}{\partial z}=-\frac{1}{\rho}\frac{\partial p}{\partial x}+\nu\nabla^2 u+F_1, \tag{2.1a}$$

$$\frac{\partial v}{\partial t}+v\frac{\partial v}{\partial y}+w\frac{\partial v}{\partial z}=-\frac{1}{\rho}\frac{\partial p}{\partial y}+\nu\nabla^2 v+F_2, \tag{2.1b}$$

$$\frac{\partial w}{\partial t}+v\frac{\partial w}{\partial y}+w\frac{\partial w}{\partial z}=-\frac{1}{\rho}\frac{\partial p}{\partial z}+\nu\nabla^2 w+F_3, \tag{2.1c}$$

$$\frac{\partial v}{\partial y}+\frac{\partial w}{\partial z}=0, \tag{2.1d}$$

where $\nabla^2\equiv(\partial^2/\partial y^2+\partial^2/\partial z^2)$, and ρ, p, ν and $\boldsymbol{F}$ are the fluid density, pressure, kinematic viscosity and a body-force respectively. The vector field $\boldsymbol{u}\equiv(u,v,w)$ depends on only two space coordinates y and z, but still has three components. Such a field is sometimes called two-and-a-half-dimensional.

Having only two independent variables, equation (2.1) can be solved either in terms of the primitive variables $(\boldsymbol{u},p)$ or by introducing the stream function defined by

$$v=\frac{\partial\psi}{\partial z},\quad w=-\frac{\partial\psi}{\partial y}, \tag{2.2}$$

and the vorticity

$$\zeta=\frac{\partial w}{\partial y}-\frac{\partial v}{\partial z}=-\nabla^2\psi. \tag{2.3}$$

Equations (2.1*b–d*) then yield

$$\frac{\partial\zeta}{\partial t}-\frac{\partial\psi}{\partial y}\frac{\partial\zeta}{\partial z}+\frac{\partial\psi}{\partial z}\frac{\partial\zeta}{\partial y}=\nu\nabla^2\zeta+\left(\frac{\partial F_3}{\partial y}-\frac{\partial F_2}{\partial z}\right). \tag{2.4}$$

To simulate the viscous sublayer, (2.1*a–d*) or (2.1*a*), (2.2–2.4) are to be solved with appropriate boundary conditions and a suitable choice of $\boldsymbol{F}$. This approach was initiated by Hatziavramidis & Hanratty (1979), and we use both their model and the variant due to Chapman & Kuhn (1980). Following Hatziavramidis & Hanratty, we have used a stream function–vorticity method, whereas Chapman & Kuhn solved the primitive $(\boldsymbol{u},p)$-equations.

2.1. *HH model*

Hatziavramidis & Hanratty (HH) proposed the following boundary conditions:

$$\psi = \zeta = 0 \quad (z = 0, \tfrac{1}{2}\lambda), \tag{2.5a}$$

$$\psi = \frac{\partial \psi}{\partial y} = 0 \quad \text{on the wall} \quad (y = 0), \tag{2.5b}$$

$$\left.\begin{aligned} u &= U_0, \\ \frac{\partial \psi}{\partial y} &= -w_{\mathrm{L}} \sin\frac{2\pi z}{\lambda} \cos \omega t, \quad \frac{\partial^2 \psi}{\partial y^2} = 0 \end{aligned}\right\} \quad (y = y_0), \tag{2.5c}$$

with $F = 0$ and the initial condition at $t = 0$

$$\psi = \frac{W_{\mathrm{L}}\lambda}{2\pi} \sin\left(\frac{2\pi z}{\lambda}\right) \frac{\sinh(2\pi y/\lambda)}{\cosh(2\pi y_0/\lambda)}, \quad \zeta = 0, \tag{2.6a}$$

$$u = U_{\mathrm{L}}(y), \tag{2.6b}$$

where $U_{\mathrm{L}}(y)$ is the velocity distribution measured by Laufer (1954). Following HH, the parameters in (2.5), (2.6) are chosen here as

$$\left.\begin{aligned} \lambda^+ &\equiv \frac{\lambda u_\tau}{\nu} = 100, \quad y_0^+ \equiv \frac{y_0 u_\tau}{\nu} = 45, \\ \omega^+ &\equiv \frac{2\pi}{T_0^+} \equiv \frac{\omega\nu}{u_\tau^2} = \frac{2\pi}{100}, \\ U_0^+ &\equiv \frac{U_0}{u_\tau} \equiv \frac{U_{\mathrm{L}}(y_0)}{u_\tau}, \quad w_{\mathrm{L}}^+ \equiv \frac{W_{\mathrm{L}}}{u_\tau} = 2.6, \end{aligned}\right\} \tag{2.7}$$

where $u_\tau \equiv (\tau_{\mathrm{w}}/\rho)^{\frac{1}{2}}$, and τ_{w} is the mean stress on the wall. HH also simulated flows with values of λ^+, y_0^+, T_{B}^+ different from (2.7). The resulting flows do not seem very different from those produced by (2.7), and we have not thought it worthwhile to make this variation.

Finite-difference methods were used to find approximate solutions of (2.1*a*), (2.2)–(2.4). The field $0 < y^+ < y_0^+$, $0 < z^+ < \lambda^+$ was divided uniformly with grid points (y_i^+, z_j^+), $i = 1, \ldots, 33$, $j = 1, \ldots, 64$, where $i = 1$ corresponds to $y^+ = 0$, i.e. the wall. By imposing fully periodic boundary conditions, the solution is made equivalent to that of HH, who solved with zero boundary conditions in the half-domain $0 < z^+ < \frac{1}{2}\lambda^+$. By using the full domain, our solution method for HH is made fully compatible with that for CK. Since we solved the equations on the ICL DAP, which has 64^2 processors, the penalty of using 64 mesh points rather than 32 in the z-direction is small.

The solution was advanced in time by applying the Adams–Bashforth scheme to the nonlinear term and the Crank–Nicholson scheme to the viscous term. Because we are interested only in the state periodic in time where the initial condition is not important, the initial condition (2.6*b*) for u was approximated by a simpler log-profile distribution. The computation was carried out on the ICL DAP (Distributed Array Processor) installed on the University of London 2980 at QMC. The root-mean-square (r.m.s.) values of the velocity field (v, w) were compared with those obtained from another code written by Dr B. A. Splawski of the QMC Turbulence Unit which uses the primitive variables (v, w) defined on a staggered mesh. No significant difference was observed.

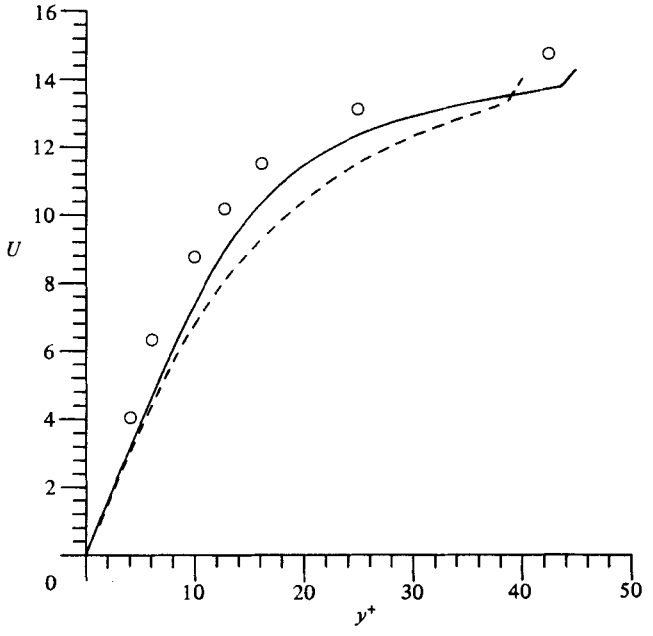

FIGURE 1. Mean-velocity profile U: ——, HH model; – – – –, CK model; ○○○, experiment by Laufer (1965).

2.2. *CK model*

Chapman & Kuhn (CK) took into account the role of the large eddies and proposed another set of the boundary conditions consisting of two components representing small and large eddies. We also tried this model. In the light of our experience, we now think that the difference between the HH model and the CK model is not crucial for the analysis discussed in the following sections. The detail of the CK-boundary condition is given in appendix A.

2.3. *Velocity field*

The mean-velocity profile $\langle u \rangle$ and the root-mean-square (r.m.s.) of $\tilde{\boldsymbol{u}} \equiv \boldsymbol{u} - \langle \boldsymbol{u} \rangle$ obtained by these HH and CK models are plotted in figures 1–3. We also plot for comparison some experimental data measured by Laufer (1954) for $Re = 50000$. All figures are presented in + units, non-dimensionalized with u_τ, ν and ρ. The 'mean average' $\langle\ \rangle$ is computed as follows:

$$\langle f \rangle = \langle \langle f \rangle_z \rangle_t, \tag{2.8}$$

where

$$\langle f \rangle_z(y) = \frac{1}{64} \sum_{j=1}^{64} f(y, z_j), \tag{2.9}$$

and $\langle\ \rangle_t$ denotes the time average over one cycle. We expect that the flow field will approach a time-periodic state after a sufficiently large time, although it is not immediately obvious that the solution of a nonlinear equation will have perfect periodicity. In computing the HH model we took the number N of the time steps per cycle to be 400. The field was observed to be almost periodic in time after a few cycles, and the time average was taken during the fifth cycle. With the CK model the period is much longer than with HH, and 3200 time steps takes us to the end of the second cycle only. Hence the average was taken during the second cycle.

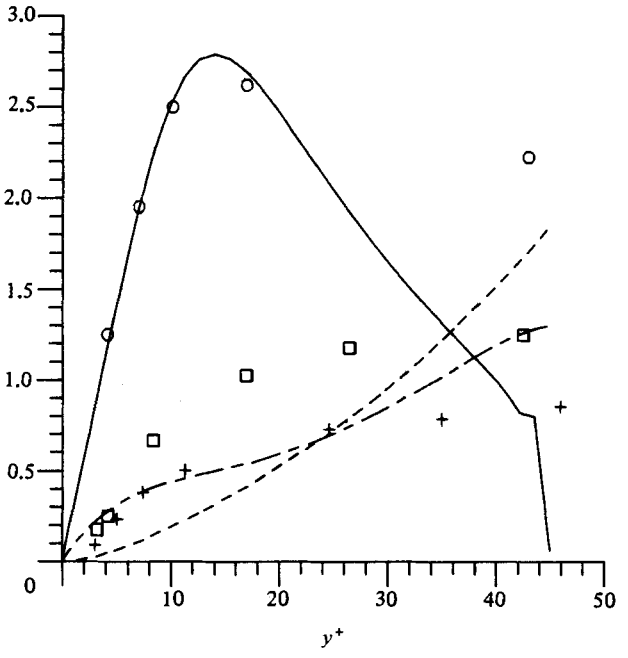

FIGURE 2. R.m.s. values of $\tilde{u}^+$, $\tilde{v}^+$ and $\tilde{w}^+$ by the HH model: ——, $\tilde{u}^+$; – – –, $\tilde{v}^+$; — — — —, $\tilde{w}^+$. Experiment by Laufer: ○○○, $\tilde{u}^+$; + + +, $\tilde{v}$; □□□, $\tilde{w}^+$.

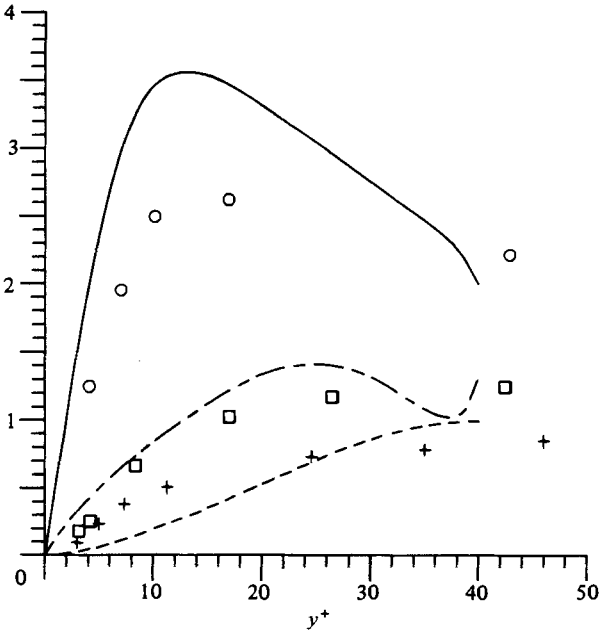

FIGURE 3. R.m.s. values of $\tilde{u}^+$, $\tilde{v}^+$, $\tilde{w}^+$ by the CK model: ——, $\tilde{u}^+$; – – –, $\tilde{v}^+$; — — — —, $\tilde{w}^+$. Experiment by Laufer; ○○○, $\tilde{u}^+$; + + +, $\tilde{v}^+$; □□□, $\tilde{w}^+$.

Results from the HH model shown in figure 1 and 2 are a little different from those reported in their paper. We think that this difference is due to an incorrect scheme used in their time-advancement procedure for the stream and vorticity functions: details are given in appendix B. The agreement between the mean-velocity profile $\langle u \rangle$ given by the HH model and that obtained by experiments (Laufer 1954) is unhappily not as good as they thought.

The slope $\mathrm{d}\langle u^+ \rangle / \mathrm{d}y^+$ of the mean velocity should be unity by definition, but the slopes given by the model calculations are not exactly unity, as may be seen in figure 1. This suggests that the boundary conditions of the models are not self-consistent. For the HH model, this slope can be easily made unity by multiplying the boundary value U_0^+ (see (2.7)) by a suitable factor (the inverse of the slope at $y^+ = 0$) and no fresh computing is needed. For CK the correction is a little more complex: again the value $\langle u \rangle$ on $y = y_0$ would then become different from the experimental value. Such corrections would not have any fundamental effect on the discussion in the following sections and we do not make them.

3. Subgrid models for the near-wall region

In large-eddy simulation (LES) a field f is decomposed into a grid scale (GS) $\bar{f}$ and a subgrid scale (SGS) f':

$$f = \bar{f} + f' \tag{3.1}$$

(see e.g. Leonard 1973; Ferziger 1981). Since the pioneering work of Deardorff (1970), there have been two substantial studies of channel flow by this method; by Schumann (1973, 1975) and Moin & Kim (1982).

3.1. *Schumann's SGS model*

We shall explain this in some detail, since we need to reproduce his procedure precisely. Schumann used the volume-balance procedure to define the resolved part $\bar{f}$ as

$$\bar{f} \equiv \frac{1}{h_1 h_2 h_3} \int_{h_1} \int_{h_2} \int_{h_3} f(z_1, z_2, z_3)\, \mathrm{d}z_1\, \mathrm{d}z_2\, \mathrm{d}z_3, \tag{3.2}$$

where h_i is the computational mesh size, and the volume over which the average is taken is fixed in space, so that $\bar{f}$ is defined only on discrete points (usually taken to be the centres of mesh volumes). Applying the filtering operation (3.2)to the Navier–Stokes equations (in this section the body force term is omitted) yields

$$\frac{\partial \bar{u}_i}{\partial t} + \sum_j \delta_j({}^j\bar{u}_j\, {}^j\bar{u}_i) = -\delta_i\, {}^i\bar{p} + \sum_j \delta_j \left(\nu \frac{\partial\, {}^j\bar{u}_i}{\partial x_j} - \overline{{}^j u_i' u_j'} \right) + p_x \delta_{ij}, \tag{3.3}$$

where $\boldsymbol{u} \equiv (u, v, w) \equiv (u_1, u_2, u_3)$, $\boldsymbol{x} \equiv (x, y, z) = (x_1, x_2, x_3)$, and ${}^j\bar{f}$ is the mean value of f averaged over the surface area ${}^jF$ of a grid volume, the normal to which is in the jth direction, e.g.

$${}^2\bar{f} \equiv \frac{1}{h_1 h_3} \int_{h_1} \int_{h_3} f(z_1, z_2, z_3)\, \mathrm{d}z_1\, \mathrm{d}z_3, \tag{3.4}$$

and

$$\delta_j\, {}^j\bar{f} \equiv \frac{\overline{{}^j \partial f}}{\partial x_j} = \frac{1}{h_j} \{ f(x_j + \tfrac{1}{2}h_j) - f(x_j - \tfrac{1}{2}h_j) \}. \tag{3.5}$$

The terms

$$\tau_{ij} \equiv \overline{{}^j u_i' u_j'} - \tfrac{1}{3}\delta_{ij} \sum_k \overline{{}^k u_k' u_k'}, \tag{3.6}$$

where

$$\overline{{}^j u_i' u_j'} \equiv \overline{{}^j (u_i - {}^j\bar{u}_i)\, (u_j - {}^j\bar{u}_j)} = \overline{{}^j \bar{u}_i\, \bar{u}_j} - {}^j\bar{u}_i\, {}^j\bar{u}_j, \tag{3.7}$$

are called SGS Reynolds stress and must be modelled.

Smagorinski (1963) suggested that the subgrid-scale stress

$$\tau_{ij} = \overline{u_i' u_j'} - \tfrac{1}{3}\delta_{ij} \sum_k \overline{u_k' u_k'} \tag{3.8}$$

should be related to the GS velocity field by an eddy-viscosity model

$$\tau_{ij} = -2\nu_n S_{ij}, \tag{3.9}$$

where

$$S_{ij} = \frac{1}{2}\left(\frac{\partial \bar{u}_i}{\partial x_j} + \frac{\partial \bar{u}_j}{\partial x_i}\right) \tag{3.10}$$

is the GS strain tensor. (This definition does not imply anyparticular form of filter.) He also proposed

$$\nu_n = C^2 h^2 \left(2 \sum_{ij} S_{ij} S_{ij}\right)^{\frac{1}{2}}, \tag{3.11}$$

where h is the mesh size (he assumed $h_1 = h_2 = h_3 = h$) and C is a non-dimensional constant subsequently found empirically to be about 0.18. Lilly (1966, 1967) justified the model in terms of turbulence theory and evaluated the constant C. He showed that, since the subgrid eddy viscosity in (3.11) is isotropic, this equation must imply isotropy of the subgrid scales. (See Leslie & Quarini (1979) for a full discussion.)

Schumann realized that near the wall there would be significant anisotropy of the subgrid scales (his 'inhomogeneous part'), and proposed a model consisting of two parts, an isotropic part which we call I and an anisotropic part which we call A, thus

$$\tau_{ij} = I_{ij} + A_{ij}, \tag{3.12a}$$

where

$$I_{ij} = -2\,{}^{ij}\mu(S_{ij} - \langle S_{ij}\rangle), \tag{3.12b}$$

$$A_{ij} = -2\,{}^{ij}\mu^* \langle S_{ij}\rangle, \tag{3.12c}$$

$$S_{ij} = \tfrac{1}{2}(\delta_i{}^j \bar{u}_j + \delta_j{}^i \bar{u}_i); \tag{3.13}$$

this being the appropriate implementation of Lilly's idea. Although Schumann defined $\langle\ \rangle$ as an ensemble average, we regard it as an average over a plane parallel to the wall, which is more appropriate in real LES. The eddy viscosity ${}^{ij}\mu$ is given by

$${}^{ij}\mu = C_2 ({}^j F\, {}^j\overline{E'})^{\frac{1}{2}}\, {}^{ij}C, \tag{3.14}$$

with

$${}^j\overline{E'} = \tfrac{1}{2} \sum_i \overline{({}^j u_i - {}^j\bar{u}_i)^2}, \tag{3.15}$$

C_2 is a constant (≈ 0.094) and ${}^{ij}C$ another constant. For turbulence whose mean flow is in the x_1 direction and which depends only on x_2, the coordinate normal to the wall, the eddy viscosity ${}^{ij}\mu^*$ is needed (and is indeed defined) for $i = 1$, $j = 2$ only. Schumann modelled it as

$${}^{12}\mu^* = ({}^2L)^2 |\delta_2 \langle u_1\rangle|, \tag{3.16}$$

$$({}^2L)^2 = \min(C_{10}^2 F, L^2), \tag{3.17}$$

$$L = 0.4 x_2, \tag{3.18}$$

where C_{10} is a constant (≈ 0.01).

3.2. *Moin & Kim's SGS model*

In their LES of a turbulent plane channel flow, Moin & Kim (1982) defined $\bar{f}$ as

$$\bar{f}(\boldsymbol{x}) = \int_p \prod_i G_i(\boldsymbol{x}, \boldsymbol{x}') f(\boldsymbol{x}')\, \mathrm{d}^3\boldsymbol{x}', \tag{3.19}$$

where G_i is the filter function in the i-direction, and the integral is extended over the whole field (Leonard 1973). In the plane parallel to the wall, in which the flow is statistically homogeneous, they used the Gaussian filter function

$$G_i(x_i, x_i') = \left(\frac{6}{\pi \Delta_i}\right)^{\frac{1}{2}} \exp\left\{-\frac{6(x_i - x_i')^2}{\Delta_i^2}\right\} \quad (i = 1, 3), \tag{3.20}$$

with $\Delta_i = 2h_i$. In the direction normal to the wall, x_2, they used a filter with a variable width $\Delta_2(x_2)$:

$$G_2(x_2, x_2') = \begin{cases} \Delta^+(x_2) + \Delta^-(x_2) & (x_2 - \Delta^-(x_2) < x_2' < x_2 + \Delta^+(x_2)), \\ 0 & (x_2' > x_2 + \Delta^+(x_2) \quad \text{and} \quad x_2' < x_2 - \Delta^-(x_2)), \end{cases} \tag{3.21}$$

with

$$\left.\begin{aligned} \Delta^+(x_2) &= \tfrac{1}{2}(x_{2j+1} - x_{2j}), \\ \Delta^-(x_2) &= \tfrac{1}{2}(x_{2j} - x_{2j-1}) \end{aligned}\right\} \quad (-\tfrac{1}{2}(x_{2j} + x_{2j-1}) < x_2 < \tfrac{1}{2}(x_{2j+1} + x_{2j})), \tag{3.22}$$

where x_{2j} is the location of the jth computational grid point in the vertical direction. The functions Δ^+ and Δ^- are thus a series of constant segments joined by jumps.

Applying the filtering operation (3.19) to the Navier–Stokes equations yields

$$\frac{\partial}{\partial t}\bar{u}_i + \sum_j \frac{\partial}{\partial x_j}\overline{\bar{u}_i \bar{u}_j} = -\frac{\partial P}{\partial x_j} + \nu \Delta \bar{u}_i - \sum_j \frac{\partial}{\partial x_j}\tau_{ij}, \tag{3.23}$$

where

$$\tau_{ij} = Q_{ij} - \tfrac{1}{3}\delta_{ij}\sum_k Q_{kk}, \tag{3.24}$$

$$P = \frac{\bar{P}}{\rho} + \tfrac{1}{3}\sum_k Q_{kk}, \tag{3.25}$$

with

$$\begin{aligned} Q_{ij} &= \overline{u_i u_j} - \overline{\bar{u}_i \bar{u}_j} \\ &= \overline{u_i' \bar{u}_j} + \overline{\bar{u}_i u_j'} + \overline{u_i' u_j'}. \end{aligned} \tag{3.26}$$

Moin & Kim's model for τ_{ij} is

$$\tau_{ij} = I_{ij} + A_{ij}, \tag{3.27a}$$

$$I_{ij} = -2\nu_T(S_{ij} - \langle S_{ij}\rangle), \tag{3.27b}$$

$$A_{ij} = -2\nu_T^*\langle S_{ij}\rangle, \tag{3.27c}$$

$$\nu_T = (C_s D\Delta)^2\left(2\sum_{i,j}(S_{ij} - \langle S_{ij}\rangle)^2\right)^{\frac{1}{2}}, \tag{3.28}$$

$$\nu_T^* = C(D^*\Delta_3)^2\left(2\sum_{i,j}\langle S_{ij}\rangle^2\right)^{\frac{1}{2}}, \tag{3.29}$$

$$C = C_s = 0.065, \tag{3.30}$$

$$\Delta = (\Delta_1 \Delta_2 \Delta_3)^{\frac{1}{3}}, \tag{3.31}$$

$$D = 1-\exp(-Y), \tag{3.32}$$

$$D^* = 1-\exp(-Y^2), \tag{3.33}$$

where $Y \equiv y_w u_\tau/25\nu$, with y_w being the distance to the nearest wall; and S_{ij} is defined by (3.13), while the meaning of $\overline{}$ is given by (3.19).

This model is similar to that of Schumann. It is, however, intended to be used in the viscous and transition layers, while Schumann's model applies to the inviscid (logarithmic) region only. Moin & Kim have therefore introduced damping factors; of Van Driest type to account for the behaviour near the wall.

3.3. *Leonard stress*

The so-called Leonard stress

$$\lambda_{ij} = \overline{\bar{u}_i \bar{u}_j} - \bar{u}_i \bar{u}_j \tag{3.34}$$

introduced by Leonard (1974) is zero for Schumann's volume balance procedure, but is not equal to zero for Moin & Kim's filtering procedure. With respect to the Gaussian filter in the horizontal directions, Moin & Kim calculated the double bar term explicitly, but with respect to the top-hat filter in the x_2 direction our understanding is that they incorporated λ_{ij} in τ_{ij}, i.e. the equation (3.27) is to be understood as a model for τ_{ij} with Q defined by

$$\begin{aligned} Q_{ij} &= \overline{u_i u_j} - \overline{\bar{u}_i \bar{u}_j} + (\overline{\bar{u}_i \bar{u}_j} - {}^{\mathrm{H}}\overline{\bar{u}_i \bar{u}_j}) \\ &= \overline{u_i u_j} - {}^{\mathrm{H}}\overline{\bar{u}_i \bar{u}_j}, \end{aligned} \tag{3.35}$$

instead of Q defined by (3.26), where ${}^{\mathrm{H}}\overline{}$ denotes the filtering in the horizontal direction only. Hereinafter we use (3.35) instead of (3.26) as the definition of Q. If the volume balance procedure is used in the x_2 direction, then (3.35) is equivalent to (3.26).†

The quantity (which we call here also Leonard stress)

$$L_{ij} = {}^{\mathrm{H}}\overline{\bar{u}_i \bar{u}_j} - \bar{u}_i \bar{u}_j, \tag{3.36}$$

is not equal to zero in Moin & Kim's procedure. Following the idea of Leonard it can be shown that

$$L_{ij} = \frac{1}{24}\left(\Delta_1^2 \frac{\partial^2}{\partial x_1^2} + \Delta_3^2 \frac{\partial^2}{\partial x_3^2}\right)(\bar{u}_i \bar{u}_j) + O(\Delta^4) \tag{3.37}$$

for the filter defined by (3.19)–(3.22). Moin & Kim showed that L_{ij} can be quite significant.

3.4. *Schumann's pseudoboundary condition*

To solve the filtered equation (3.3) or (3.23) we need the boundary condition for

$$\nu \frac{\partial^2 \bar{u}_1}{\partial x_2} \text{ in (3.3)} \quad \text{or} \quad \nu \frac{\partial \bar{u}_i}{\partial x_2} \text{ in (3.23).} \tag{3.38}$$

Moin & Kim used natural boundary conditions with a fine mesh near the wall. Then $\nu\,\partial\bar{u}_1/\partial x_2$ can be represented in the usual way. This approach is obviously satisfactory in principle. In practice it suffers from a shortage of mesh points. It is not certain that the finest mesh now available is sufficient even at low Reynolds number.

† We are here reporting what we understand Moin & Kim to have done. We note that the QMC group has reservations about the whole concept of filtering (Antonopoulos-Domis 1981).

Realizing that the mesh is not sufficiently fine in his LES, Schumann introduced an assumption

$$\tau_w \equiv \nu \frac{\partial^2 \bar{u}_1}{\partial x_2}\bigg|_{\text{wall}} = \frac{{}^1\bar{u}_1}{\langle {}^1\bar{u}_1 \rangle}\bigg|_1 \langle \tau_w \rangle, \tag{3.39}$$

where the subscript 1 denotes that the quantity is to be evaluated at the grid adjacent to the wall. The brackets $\langle\ \rangle$ is here regarded as the mean average over time and the plane parallel to the wall.

4. Testing of models in LES

4.1. *Test procedure*

We will now use fields generated from the 2.5-dimensional model fields set out in §2 to analyse the various models for the subgrid stress in the near-wall region described in §3.

The filtered quantities $\bar{u}_i$, $\overline{u_i' u_j'}$ etc. used in the definition of the subgrid stress can be computed from the 2.5-dimensional model fields available on the 33×64 grid points distributed uniformly over the (y^+, z^+)-plane. We can also compute these stresses according to the SGS models set out in §3, using filtered quantities obtained from the 2.5-dimensional realizations. In this section, 'experimental' or 'exp' refers to numerical experimental values computed from the HH- or CK-model fields,as described in §2.

For the comparison we define a coarse grid of points Y_I (or x_{2I}), $I = 1, 2, 3, \ldots$, in the y-direction in accordance with Moin & Kim's scheme, by

$$Y_I^+ \equiv \frac{Y_I}{\nu/u_\tau} = \left(\frac{1}{a}\tanh\{\xi_I \tanh^{-1}(a)\} + 1\right) Re_\delta, \tag{4.1}$$

with $\xi_I = -1 + 2(I-1)/62$, $a = 0.98346$. (In this paper we put $Re_\delta = 640.25$ and $Y_1^+ = 0$, $Y_2^+ \approx 1.78, \ldots, Y_{11}^+ \approx 38.18$, $Y_{12}^+ \approx 45.99$.)The mesh width h_3 of the LES grid in the 3-direction is independent of the y-coordinate, as it was in the Moin–Kim simulation. Because our 'experimental' fields are independent of x, the filtering operation in the x-direction is perforce omitted.

In this work, the trapezoidal rule is used to evaluate the integrals in the filtering procedure, other than the x_3 integrals in (3.19): these are evaluated in wavenumber space. When a value of ${}^2\tilde{f}(y)$ (see (3.4)) is needed at a y-value away from the points of the representational grid, it is computed by first calculating the velocity at the appropriate y-value by interpolation and then performing the filtering operation. The z-average $\langle f \rangle$ (y) is obtained by first computing $\tilde{f}$ on (y, z_j), $j = 1, \ldots, 64$, and then taking the z-average in accordance with (2.9). The mean average $\langle\ \rangle$ is computed in the same way as (2.8).

4.2. *Modelling of the subgrid Reynolds stress: definition and procedures*

Let us first consider τ_{12}, the most important component of τ_{ij} in determining the mean-velocity profile $\langle u_1 \rangle$. We will now compare 'experimental' values of the subgrid stress τ_{12} with those given by Schumann's or Moin & Kim's model, using 'experimental' values of the filtered velocities to evaluate the model stresses. The quantities τ_{12}, I_{12} and A_{12} (see (3.12) and (3.27)) so evaluated are here called τ_{mod}, I_{mod} and A_{mod} respectively. The reader is asked to note that 'mod' now refers to quantities computed from the 'experimental' velocity field according to the subgrid model.

Because the HH- and CK-model field have no $x(x_1)$ dependence, we modify ${}^2\overline{F}$ in (3.14), (3.17) and Δ in (3.31) from ${}^2\overline{F} = h_1 h_3$, $\Delta = (\Delta_1\Delta_2\Delta_3)^{\frac{1}{3}}$ to

$$ {}^2\overline{F} = (h_3)^2, \quad \Delta = (\Delta_2\Delta_3)^{\frac{1}{2}}, \tag{4.2a, b} $$

and put ${}^{12}C = 1$. (Instead of (4.2*b*) we could have used

$$ \Delta = \{(\Delta_2)^2 + (\Delta_3)^2\}^{\frac{1}{2}} \quad \text{or} \quad \Delta^{-1} = \{(\Delta_2)^{-2} + (\Delta_3)^{-2}\}^{\frac{1}{2}}.) $$

Since the mesh width in the y-direction is not distributed uniformly, the question of how to approximate the y-derivatives appearing in LES modelling is not trivial. The derivatives in (3.12) were computed as

$$ \delta_2\langle u_1\rangle_z(Y_I, z) = \left\langle \frac{u_1(Y_{I+1}, z) - u_1(Y_{I-1}, z)}{Y_{I+1} - U_{I-1}} \right\rangle, \tag{4.3} $$

$$ 2S_{12}(Y_I, z) = \delta_2\,{}^1\overline{u} = \frac{u_I(z) - u_{I-1}(z)}{Y_{I+\frac{1}{2}} - Y_{I-\frac{1}{2}}}, \tag{4.4} $$

where

$$ u_I(z) = \frac{1}{Y_{I+1} - Y_I}\int_{Y_I}^{Y_{I+1}}\int_{h_3} u(y', z')\,dy'\,dz', \tag{4.5} $$

and Y_I is defined by (4.1). The derivatives in(3.27) were computed as

$$ \frac{\partial f}{\partial y}(Y_I) = \frac{f(Y_{I+1}) - f(Y_{I-1})}{Y_{I+1} - Y_{I-1}}, \tag{4.6} $$

$$ \frac{\partial f}{\partial z}(z_j) = \frac{f(z_j + h_3) - f(z_j - h_3)}{2h_3}. \tag{4.7} $$

The 'experimental' fields are known only for $0 < y^+ < 45$ (HH model) or $0 < y^+ < 40$ (CK model), and the formulae can be applied at interior points only. Moreover the values at the last one or two interior points are unreliable. Derivatives at such points were not computed and do not appear on the figures. This accounts for the truncated appearance of some diagrams.

The subgrid stress τ_{12} can be decomposed into the z-average $\langle\tau_{12}\rangle_z$ and the deviation $\tau_{12} - \langle\tau_{12}\rangle_z$ from the z-average. We call the 'experimental' values of τ_{12}, $\langle\tau_{12}\rangle_z$ and $\tau_{12} - \langle\tau_{12}\rangle_z$ τ_{exp}, A_{exp} and I_{exp} respectively, so that

$$ \tau_{\text{exp}} = A_{\text{exp}} + I_{\text{exp}}, \tag{4.8} $$

$$ \langle\tau_{\text{exp}}\rangle_z \equiv A_{\text{exp}}, \quad \tau_{\text{exp}} - \langle\tau_{\text{exp}}\rangle_z \equiv I_{\text{exp}}. \tag{4.9a, b} $$

For both the Schumann and the Moin & Kim models, $A_{\text{mod}} = \langle A_{\text{mod}}\rangle_z$, and we therefore have

$$ \langle\tau_{\text{mod}}\rangle_z = A_{\text{mod}} + \langle I_{\text{mod}}\rangle_z, \tag{4.10a} $$

$$ \tau_{\text{mod}} - \langle\tau_{\text{mod}}\rangle_z = I_{\text{mod}} - \langle I_{\text{mod}}\rangle_z, \tag{4.10b} $$

because the eddy viscosities ${}^{12}\mu^*$, ν_{T}^* for the anisotropic part are independent of z. (Note that the brackets $\langle\ \rangle$ in (3.12) denote the z-average which is our approximation to an average over the (x, z)-plane.) If the z-dependence of the eddy viscosities ${}^{12}\mu$, ν_{T} for the isotropic part is negligible, then $\langle I_{\text{mod}}\rangle_z = 0$, and (4.10) exactly corresponds to (4.9). In this sense, A_{mod} and I_{mod} may be roughly regarded as the models for A_{exp} and I_{exp} respectively.

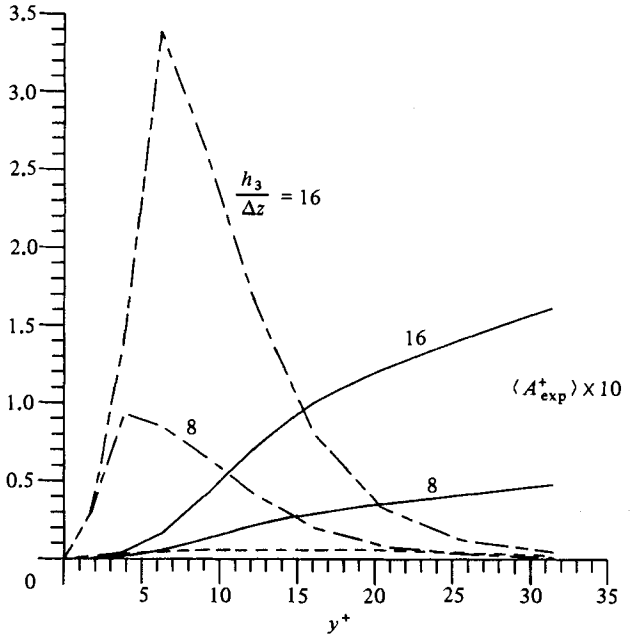

FIGURE 4. $\langle A^+_{exp}\rangle$, $\langle A^+_{mod}\rangle$ and $\langle I^+_{mod}\rangle$ for Schumann's LES. HH model. ——, $\langle -A^+_{exp}\rangle \times 10$; ————, $\langle -A^+_{mod}\rangle$; ---, $\langle -I^+_{mod}\rangle$.

4.3. *Modelling of the subgrid Reynolds stress: results*

Now let us compare the *averages* of τ_{exp} and τ_{mod}. From (4.9a) and (4.10a), we have

$$\langle \tau_{exp}\rangle = \langle A_{exp}\rangle, \quad \langle \tau_{mod}\rangle = \langle A_{mod}\rangle + \langle I_{mod}\rangle. \tag{4.11}$$

In figure 4 are plotted the values of $\langle A_{exp}\rangle$, $\langle A_{mod}\rangle$ and $\langle I_{mod}\rangle$ computed from HH-model fields for Schumann's definition of subgrid stress (3.6) and his model (3.12). The filter width h_3 in the z-direction is chosen as $h_3^+ = 8(\Delta z^+)$ or $h_3^+ = 16(\Delta z^+)$, where $\Delta z^+ \equiv \lambda^+/64 = 100/64$ is the mesh width in the z-direction of the fine grid system. In figure 5 are plotted the values for Moin & Kim's definition of subgrid stress (3.24) and for their model (3.27). It is found that the value of $|\langle I_{mod}\rangle|$ is very much smaller than that of $|\langle A_{mod}\rangle|$ and therefore $\langle \tau_{mod}\rangle \approx \langle A_{mod}\rangle$; this is in accordance with our expectation. In Schumann's modelling the value of $|\langle I_{mod}\rangle|$ for $h_3^+ = 8(\Delta z^+)$ is smaller than that for $h_3^+ = 16(\Delta z^+)$ and is not included in figure 4. In Moin & Kim's model, values of $|\langle I_{mod}\rangle|$ for both $h_3^+ = 8(\Delta z^+)$ and $16(\Delta z^+)$ are too small to be plotted in figure 5.

In Schumann's model (3.12), the magnitude of $\langle A_{mod}\rangle$ is proportional to

$$(\delta_2 \langle u_1\rangle)^2. \tag{4.12}$$

Very close to the wall ($y^+ \lesssim 10$), the slope $\partial\langle u\rangle/\partial y$ is very high (cf. figure 1). Hence it is not surprising that $|\langle A_{mod}\rangle|$ is very high near $y^+ \approx 5$ as seen in figure 4. The agreement between Schumann's $\langle A_{mod}\rangle$ and $\langle A_{exp}\rangle$ is very poor. Schumann's SGS model was not intended for use in the near-wall region, and in a sense it is unfair to apply it there: none the less, the results seem interesting enough to record. The SGS model should be valid in the logarithmic region, and the disagreement there is disquieting. At the moment. we cannot say whether the error is in the model or is due to the deviation of the 2.5-dimensional velocity fields from the actual behaviour of near-wall turbulence.

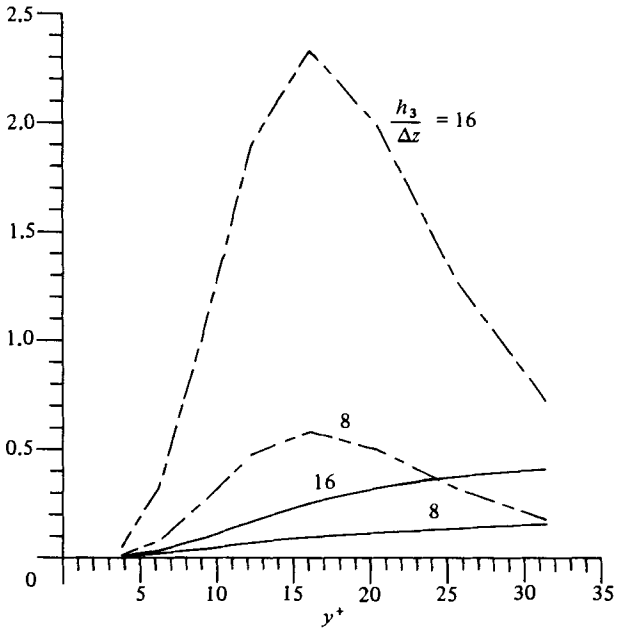

FIGURE 5. $\langle A^+_{\rm exp}\rangle$ and $\langle A^+_{\rm mod}\rangle$ for Moin & Kim's LES. HH model. ——, $\langle -A^+_{\rm exp}\rangle$; – – – – –, $\langle -A^+_{\rm mod}\rangle$.

Such a disagreement or ill-behaviour of $\langle A_{\rm mod}\rangle$ is significantly modified in Moin & Kim's model (3.27) by the introduction of the factor D^* defined by (3.33). However, the agreement between $\langle A_{\rm mod}\rangle$ and $\langle A_{\rm exp}\rangle$ is still not satisfactory. From (3.27) and (3.29), $\langle A_{\rm mod}\rangle$ is to be proportional to $\Delta_3^2 \equiv (2h_3)^2$; figure 5 suggests that the dependence of $\langle A_{\rm exp}\rangle$ is not nearly as strong as this. It may be interesting to note that the order of magnitude of $\langle A_{\rm mod}\rangle$ is similar to that of $\langle A_{\rm exp}\rangle$ especially for $h_3 = 8\Delta_3$, i.e. $h_3^+ = 12.5$ in figure 5. This justifies to some extent Moin & Kim's choice of the value 0.065 for C in (3.30). (In their LES, they used $h_3^+ = 15.7$ and 20.9.) However, if the 2.5-dimensional velocity field is anywhere near correct, the SGS model is in need of substantial modification.

Next we compare the deviations $\tau_{\rm exp} - \langle\tau_{\rm exp}\rangle_z$ and $\tau_{\rm mod} - \langle\tau_{\rm mod}\rangle_z$, i.e. $I_{\rm exp}$ and $\tilde{I}_{\rm mod} \equiv I_{\rm mod} - \langle I_{\rm mod}\rangle_z$. It is clear from (4.9*b*) and (4.10*b*) that $\langle I_{\rm exp}\rangle = \langle \tilde{I}_{\rm mod}\rangle = 0$. The r.m.s. values of $I_{\rm exp}$ and $\tilde{I}_{\rm mod}$ are plotted for Schumann's definitions and SGS model in figure 6 and for Moin & Kim's definitions and SGS model in figure 7. Again the agreement between the experimental values and the values given by the models is not very good in both cases. The Schumann SGS model is of the right order of magnitude, but it peaks too near the wall. This is not surprising, since it does not include a wall correction. The r.m.s. values of $\tilde{I}_{\rm mod}$ in Moin & Kim's model is wrong by three orders of magnitude.

We have also computed the correlation C_I between $I_{\rm exp}$ and $\tilde{I}_{\rm mod}$:

$$C_I(y) = \frac{\langle I_{\rm exp}\tilde{I}_{\rm mod}\rangle}{(\langle (I_{\rm exp})^2\rangle \langle (\tilde{I}_{\rm mod})^2\rangle)^{\frac{1}{2}}}. \tag{4.13}$$

The value of C_I is not affected by the choices of the values of C_2, ^{12}C, $C_{\rm s}$ or ^2F, D used in the models. In figure 8 are plotted the values of C_I obtained from the HH model for $h_3/\Delta z = 8$ and 16. In Schumann's model, C_I lies between 0.5 and 0.7. In view of the experience of Clark *et al.* (1979) this is modestly encouraging. In Moin

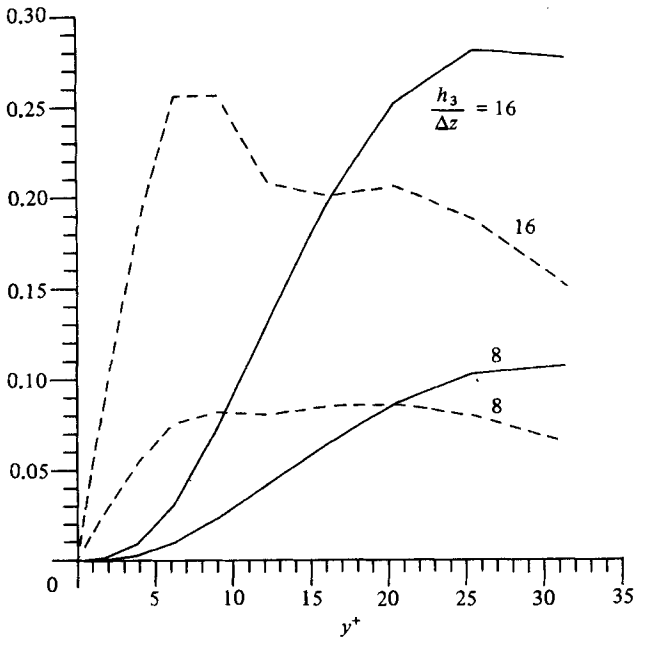

FIGURE 6. R.m.s. values of I^+_{exp} and $\bar{I}^+_{mod}$ for Schumann's LES: ——, I^+_{exp}; – – –, $\bar{I}^+_{mod}$. HH model.

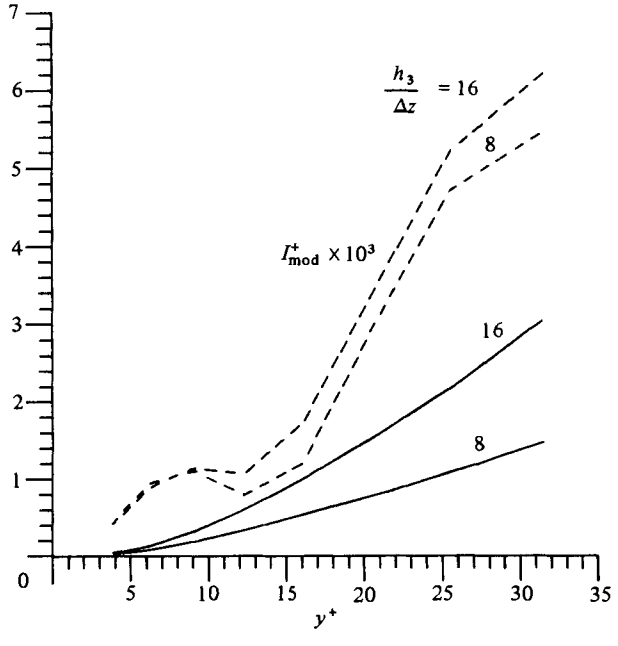

FIGURE 7. R.m.s. values of I_{exp} and $\bar{I}^+_{mod}$ for Moin & Kim's LES. ——, I^+_{exp}; – – –, $\bar{I}^+_{mod} \times 10^3$. HH model.

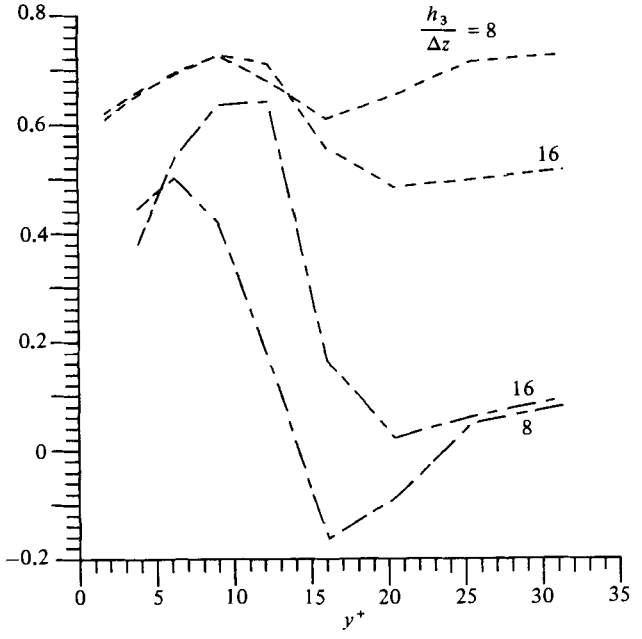

FIGURE 8. Correlation between I^+_{exp} and $\tilde{I}^+_{\text{mod}}$. HH model. ——, Schumann's LES; – – – – –, Moin & Kim's LES.

& Kim's model the value of C_I is disappointingly low: in some regions it is actually negative.

Similar comparisons between $\langle \tau_{\text{mod}} \rangle$ and $\langle \tau_{\text{exp}} \rangle$ and between $\tau_{\text{mod}} - \langle \tau_{\text{mod}} \rangle_z$ and $\tau_{\text{exp}} - \langle \tau_{\text{exp}} \rangle$ have also been made with 2.5-dimensional velocity fields generated from the CK model. The results do not show significant qualitative differences from those given by the HH model, except for the value of the correlation coefficient C_I for Schumann's model which is shown in figure 9; this value is not as high in the CK model as in the HH model. Otherwise, we present here (in figure 10) only the result of the comparison between $\langle A_{\text{exp}} \rangle$, $\langle A_{\text{mod}} \rangle$ and $\langle I_{\text{mod}} \rangle$ for the Schumann definition and model, which corresponds to figure 4 for the HH model.

4.4. *Pseudopressure and subgrid energy*

The pressure computed in an LES is the P defined by (3.25) for Moin & Kim's scheme and by a similar one (not given here) for Schumann's scheme. It is therefore a pseudo-pressure, and it magnitude is affected by a contribution from the subgrid velocity energy (the Q-term in (3.25) for Moin & Kim's scheme). We have used our modelling technique to investigate the importance of this contribution.In figures 11 and 12 are compared the average $\langle p \rangle$ of the 'true' pressure and the contribution $R \equiv \frac{1}{3} \sum_k Q_{kk}$ from the subgrid velocity energy as given by the HH model, where Q_{kk} is defined by (3.35) for Moin & Kim's scheme and $Q_{kk} \equiv {}^2\overline{u_k u_k} - {}^2\overline{u_k}\,{}^2\overline{u_k}$ for Schumann's scheme. As can be seen in the figures, the contribution R is not negligibly small when compared to $\langle p \rangle$, especially for smaller y^+ and/or larger h_3, i.e. $h_3 = 16\Delta z$. The results obtained for the CK model are qualitatively similar.

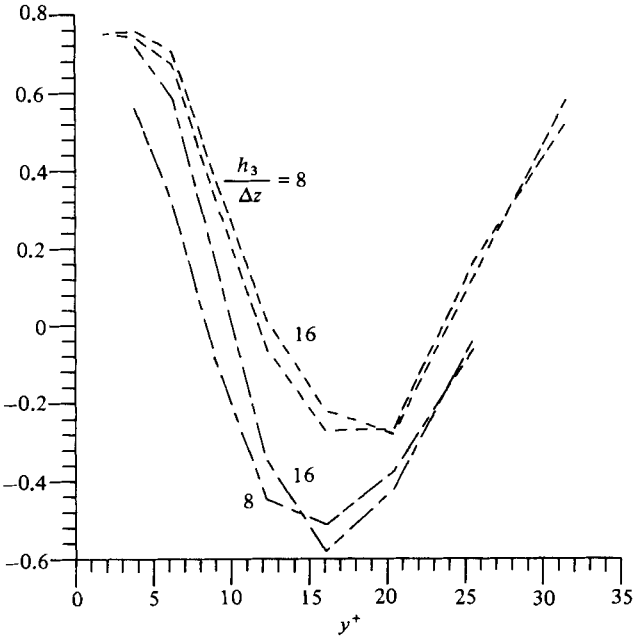

FIGURE 9. Same as in figure 8, but by the CK model.

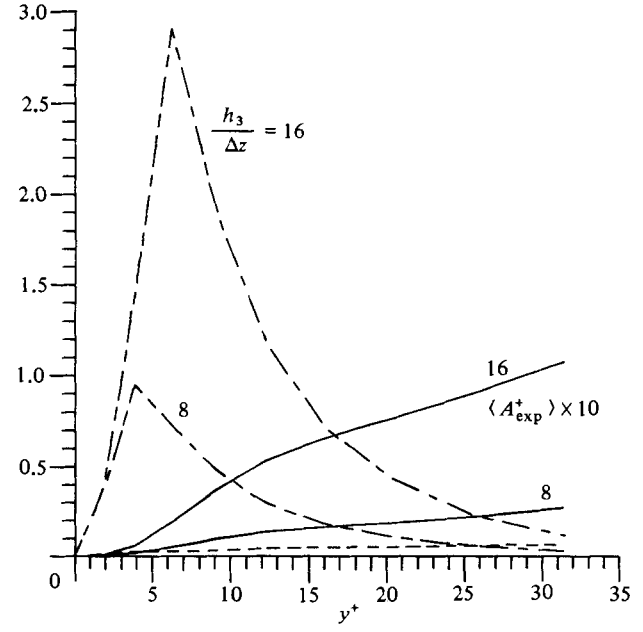

FIGURE 10. Same as in figure 4, but by the CK model.

4.5. *The Leonard stress*

We denote the experimental value of L_{12} defined by (3.36) as $L_{\rm exp}$. Because our 'experimental' velocity field is independent of x_1, the Leonard model (3.27) yields

$$L_{12} = \tfrac{1}{24}\Delta_3^2 \frac{\partial^2}{\partial x_3}(\overline{uv}), \tag{4.14}$$

where the term $O(\Delta^2)$ in (3.37) is omitted. We denote the value of L_{12} given by

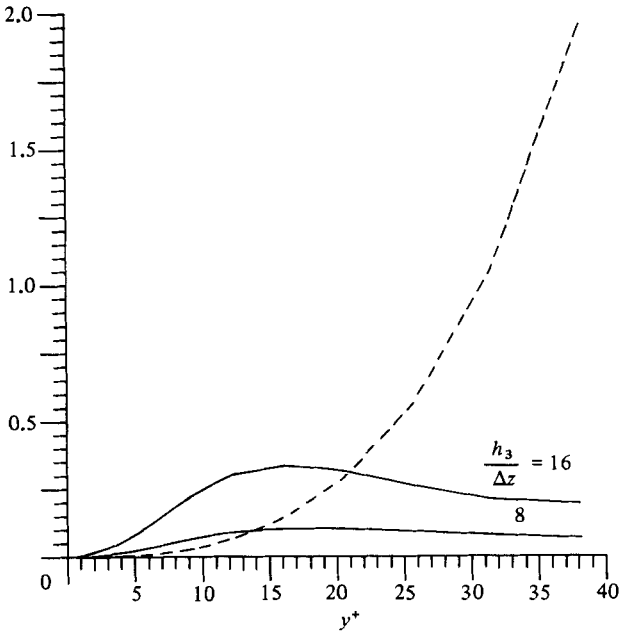

FIGURE 11. The averages of the pressure p^+ and the contribution R from the subgrid energy to the pseudopressure. HH model. Schumann's LES. ——, $\langle R^+ \rangle$; – – –, $\langle -p^+ \rangle$.

the model (4.14) as L_{mod}. It is clear that $\langle \overline{\bar{u}\bar{v}} \rangle_z = \langle \bar{u}\bar{v} \rangle_z$ and therefore $\langle L_{\text{exp}} \rangle_z = \langle L_{\text{exp}} \rangle = 0$, and that, because of the periodicity in the z-direction of our 'experimental' field, $\langle L_{\text{mod}} \rangle = 0$ also.

The r.m.s. value of L_{mod} was found to be very close to that of L_{exp} with both the HH model and the CK model. The r.m.s. values obtained from the HH model are plotted in figure 13 for $h_3/\Delta z = 8$ and 16. The correlation between L_{exp} and L_{mod} is found to be also very satisfactory; it is found to be larger than 0.99 in both CK and HH models for $y = Y_I$ ($I = 2, \ldots, 11$). Since Leonard's model for the Leonard stress seems reasonable, the model L_{mod} was expected to represent L_{exp} rather well, but the agreement is much better than we had expected.

4.6. *Schumann's pseudoboundary condition*

So far as the mean value is concerned, the assumption (3.39) is clearly consistent, i.e.

$$\langle \tau_{\text{w}} \rangle = \langle \tau_2^{\text{mod}} \rangle, \tag{4.15}$$

where $\tau_{\text{w}}^{\text{mod}}$ is the model of τ_{w} represented by the right-hand-side term of (3.39). We decompose τ_{w} and $\tau_{\text{w}}^{\text{mod}}$ into mean and fluctuating parts as

$$\left.\begin{aligned} \tau_{\text{w}} &= \langle \tau_{\text{w}} \rangle + \tilde{\tau}_{\text{w}} = \langle \tau_{\text{w}} \rangle (1+r), \\ \tau_{\text{w}}^{\text{mod}} &= \langle \tau_{\text{w}}^{\text{mod}} \rangle + \tilde{\tau}_{\text{w}}^{\text{mod}} = \langle \tau_{\text{w}} \rangle (1+r_{\text{mod}}), \end{aligned}\right\} \tag{4.16}$$

where (4.15) has been used. The fluctuating part $\tilde{\tau}_{\text{w}}^{\text{mod}}$ depends on the size of the coarse grid adjacent to the wall and we need to define this size in order to compare τ_{w} and $\tau_{\text{w}}^{\text{mod}}$. We have taken the coarse grid in the y-direction next to the wall ($y^+ = 0$) to be as large as $y^+ = \Delta y^+ \times 22$ (≈ 30.9 in HH model, ≈ 27.5 in CK model).

In table 1 are shown the values of the correlation C_τ between τ_{w} and $\tau_{\text{w}}^{\text{mod}}$, the correlation C_r between r and r_{mod}, and the r.m.s. values of r and r_{mod}. As can be seen,

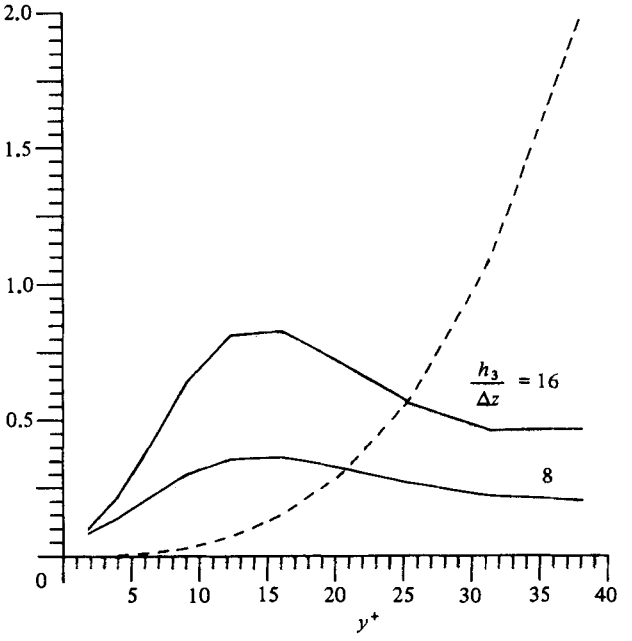

FIGURE 12. Same as in figure 10, but for Moin & Kim's LES. ——, $\langle R^+ \rangle$; – – –, $\langle -p^+ \rangle$.

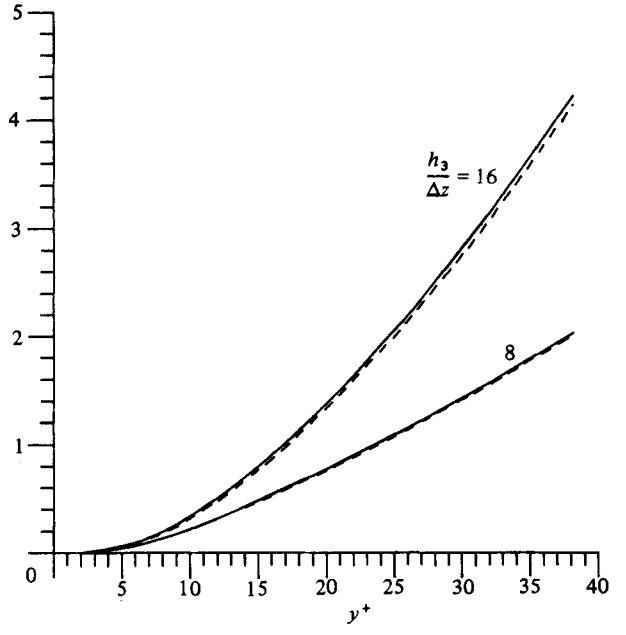

FIGURE 13. Comparison of the r.m.s. value of the Leonard model L_{mod} with that of the Leonard stress L^+_{exp}. ——, L^+_{exp}; – – –, L^+_{mod}.

	HH model		CK model	
	$\frac{h_2}{\Delta z} = 8$	16	8	16
C_τ	0.98	0.98	0.94	0.94
C_r	0.82	0.82	0.88	0.89
r.m.s. r	0.36	0.36	0.70	0.70
r.m.s. r_{mod}	0.21	0.19	0.36	0.35

TABLE 1

the values of both C_τ and C_r are quite high. This suggests that the stress τ_w on the wall is well correlated with the flux ${}^1\bar{u}_1$ averaged over the grid adjacent to the wall, and is therefore well represented by the model (3.39).

5. Testing of k, ϵ model

The model fields generated in §2 could be used for testing the standard one-point closures.

Let us write

$$\left.\begin{aligned} \boldsymbol{u} &= \boldsymbol{U}+\tilde{\boldsymbol{u}}, \quad \mathrm{U} \equiv \langle \boldsymbol{u} \rangle, \\ \frac{p}{\rho} &= P+\tilde{p}, \quad P \equiv \frac{\langle p \rangle}{\rho}, \\ k &= \tfrac{1}{2}\langle \tilde{\boldsymbol{u}}\tilde{\boldsymbol{u}} \rangle. \end{aligned}\right\} \tag{5.1}$$

Then it is a standard result that

$$\frac{\partial}{\partial t} U_i + U_j \frac{\partial U_i}{\partial x_j} = -\frac{\partial P}{\partial x_i} - \frac{\partial}{\partial x_j}\langle \tilde{u}_i \tilde{u}_j \rangle + \nu \nabla^2 U_i, \tag{5.2}$$

$$\frac{\partial}{\partial t} k + U_j \frac{\partial k}{\partial x_j} = \mathscr{P} - \epsilon + \mathscr{D}, \tag{5.3}$$

where

$$\left.\begin{aligned} \mathscr{P} &= -\langle u_i u_j \rangle \frac{\partial U_i}{\partial x_j}, \quad \epsilon = 2\nu \bar{S}_{ij} \bar{S}_{ij}, \\ \mathscr{D} &= \frac{\partial}{\partial x_j}\left(-\langle \tilde{p}\tilde{u}_i \rangle \delta_{ij} - \tfrac{1}{2}\langle \tilde{u}_i \tilde{u}_i \tilde{u}_j \rangle + \nu \left\{ \frac{\partial k}{\partial x_i} + \frac{\partial}{\partial x_i}\langle \tilde{u}_i \tilde{u}_j \rangle \right\} \right), \\ \nabla^2 &= \frac{\partial}{\partial x_i}\frac{\partial}{\partial x_i}, \quad \bar{S}_{ij} = \frac{1}{2}\left(\frac{\partial \tilde{u}_j}{\partial x_i} + \frac{\partial \tilde{u}_i}{\partial x_j} \right), \end{aligned}\right\} \tag{5.4}$$

and the summation convention is used for repeated indices in this section only. Equations may also be formulated for the $\langle \tilde{u}_i \tilde{u}_j \rangle$ appearing in (5.2). Various approximation methods have been developed for solving these equations: see, for example, Launder & Spalding (1972).

The turbulent energy k and the energy dissipation ϵ play a crucial role in the most popular of these approximations, and it is interesting to see their behaviour in the

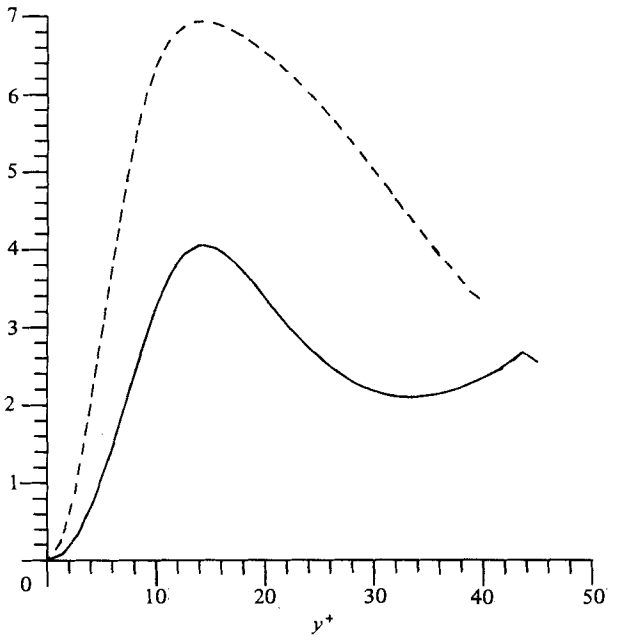

FIGURE 14. Turbulent energy k^+: ——, HH model; – – –, CK model.

2.5-dimensional models. The dependences of k and ϵ on y in these models are shown in figures 14 and 15. We also plot

$$\epsilon' \equiv \epsilon - 2\nu\left(\frac{\partial k^{\frac{1}{2}}}{\partial y}\right)^2 \tag{5.5}$$

as a possible representation of the turbulent (high-wavenumber) dissipation. There are computational advantages in using ϵ' instead of ϵ, because ϵ' is zero on the wall. Jones & Launder (1972, 1973) made the transformation (5.5) for purely computational reasons, but it could also be interpreted as the high-wavenumber part of the dissipation (Leslie, unpublished). As is seen in these figures ϵ_{mod} and k_{mod} have their peaks near $y^+ \approx 10$, where as is well known the turbulence production is most intense. The rather odd behaviour near the outer edge is presumably due to the failure of the 2.5-dimensional model in this region. We note that ϵ' is indeed small near the wall, so that the Jones–Launder model achieves its objective.

We have used these fields to compute the length-scales

$$l = 0.164\frac{k^{\frac{3}{2}}}{\epsilon}, \quad l' = 0.164\frac{k^{\frac{3}{2}}}{\epsilon'}, \tag{5.6}$$

both of which should be equal to $0.4y^+$ in the logarithmic region. The results, shown in figure 16, are disappointing, l failing to show the required linear increase with y in the outer regions of the simulation. We had proposed to use the 2.5-dimensional fields to test models for the various terms in the k- and ϵ-equations, but it now seems to us that the process for generating the 'experimental' velocity fields must be improved if this exercise is to have any practical value.

After we have obtained these results, Professor Hanratty remarked to us that his model was not intended for use outside the viscous wall region.

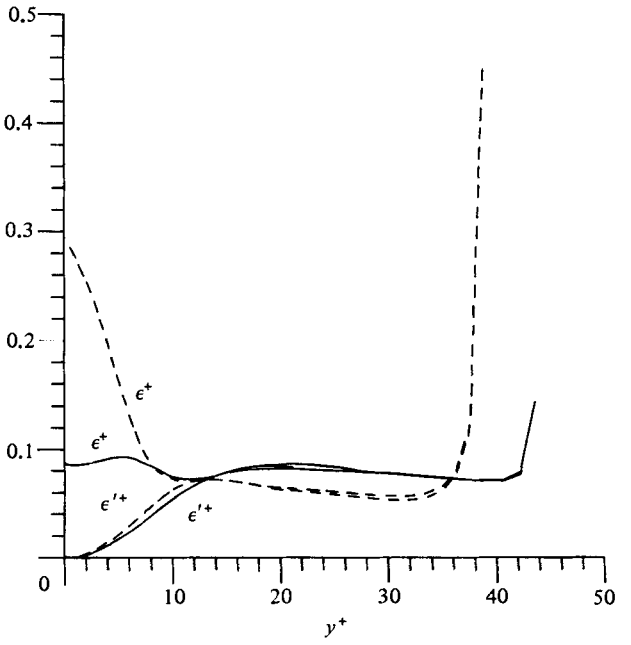

FIGURE 15. Turbulent-energy dissipation ϵ^+ and ϵ'^+: ——, HH model; – – –, CK model.

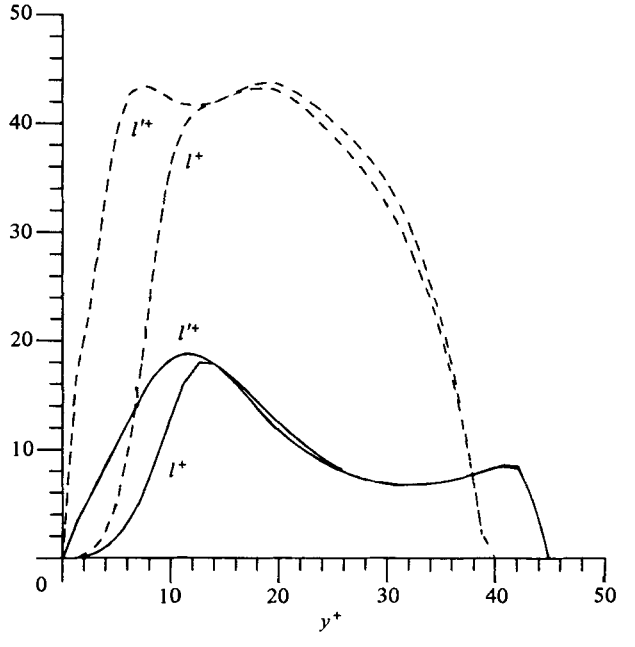

FIGURE 16. The lengthscales l^+ and l'^+ defined by (5.6): ——, HH model; – – –, CK model.

6. Discussion and conclusions

The 2.5-dimensional model introduced by HH and improved by CK is, so far as we know, the first procedure for generating reasonably realistic near-wall velocity fields: we have used it to test the subgrid models proposed by Schumann and by Moin & Kim. The results are as follows.

(i) The models for $\langle A \rangle$ (roughly the r.m.s. subgrid Reynolds stress) are bad: both show large peaks near the wall which are quite absent from the 'true' or 'experimental' fields.

(ii) The r.m.s. fluctuations of the isotropic part are much better predicted. The Schumann model peaks too near the wall but is of the right order of magnitude: the Moin–Kim model has the right trend with y^+ but its magnitude is wrong by three orders of magnitude. The correlation between I_{mod} and I_{exp} is quite reasonable for the Schumann model and HH fields, but very poor with the Moin & Kim model.

(iii) We have calculated the contribution R of the subgrid energy to the pseudo-pressure which appears in the LES equations of motion. The contribution R is found to be non-negligible compared to the pressure, for small y and/or larger filter width.

(iv) Leonard's model represents the Leonard stress very well. The r.m.s. value of the model is very close to that of the actual Leonard stress and the correlation between the model and the stress is very close to unity.

(v) The most important positive result of this investigation is that Schumann's synthetic boundary condition (3.39), which has been criticized, is in fact extremely good: τ_{w} is closely correlated with u outside the viscous layer. The present experiment of Robinson (1982) shows exactly the same effect, and this provides encouraging confirmation that the 2.5-dimensional velocity fields are, in this respect at least, not too far from reality.

(vi) For the purpose of this paper, there is little difference between the original HH formulation of the 2.5-dimensional field-generation procedure and the later, more sophisticated version due to CK.

If these results are taken at their face value, they imply that the subgrid models are in need of substantial improvement. This conclusion must be taken with more than a grain of salt, since the results in §5 suggest that the velocity fields generated by the existing 2.5-dimensional procedures may not be accurate enough for this rather delicate work. These procedures need to be improved, and our investigations (not reported above) suggest that the modifications will have to be fairly radical.

We are grateful to Dr B. A. Splawski of the Department of Nuclear Engineering at QMC for substantial help with code preparation and to Professor Hanratty for the remark noted at the end of §5. Y. Kaneda is indebted to the British SERC for a maintenance grant and to the Japanese Ministry of Education for a travel scholarship.

Appendix A. CK boundary conditions

Chapman & Kuhn (CK) have proposed a model somewhat more complicated than that of HH, in which besides the obvious boundary condition on the wall

$$\boldsymbol{v} = 0 \quad (y = 0) \tag{A 1}$$

and the periodic side boundary condition

$$\boldsymbol{v}(y, 0, t) = \boldsymbol{v}(y, \lambda, t), \tag{A 2}$$

the following boundary conditions are assumed on the outer edge $y = y_0$:

$$u^+ \equiv \frac{u}{u_\tau} = U_e + 2\alpha_1 \sin(N_1 t^+) \sin\xi + (2(\alpha^2 - \alpha_1^2))^{\frac{1}{2}} \sin(N_{u2} t^+ + \phi_{u2}), \quad \text{(A 3}a\text{)}$$

$$v^+ \equiv \frac{v}{u_\tau} = -2\beta \sin(N_1 t^+) \sin\xi, \quad \text{(A 3}b\text{)}$$

$$w^+ \equiv \frac{w}{u_\tau} = 2\beta \cos(N_1 t^+) \cos\xi + (2(\gamma^2 - \beta^2)^{\frac{1}{2}} \sin(\tfrac{1}{2} N_{u2} t^+ + \phi_{w2}), \quad \text{(A 3}c\text{)}$$

where

$$t^+ \equiv \frac{t u_\tau^2}{\nu}, \quad \xi \equiv \frac{2\pi}{\lambda}\left(\frac{z u_\tau}{\nu}\right),$$

$$\alpha = 2.0, \quad \beta = 1.0, \quad \gamma = 1.3, \quad \alpha_1 = -0.45\alpha,$$

$$\lambda = 100, \quad y_0^+ = \frac{y_0 u_\tau}{\nu} = 40.0.$$

Some points are not fully explicit in their paper and we have found it difficult to reproduce their results. These points are as follows.

(i) *The mean flow part U_e in* (A 3*a*). This term is not included in their boundary condition. However, if their (12) or (21) (which is equivalent to our (2.1)) is to be used as a basic equation, this term should be included. We do so, and put

$$U_e = 2.6 + 5.2 \ln y_0^+ \approx 14.7 \quad \text{(A 4)}$$

(this being the value given by the standard logarithmic formula).

(ii) *The values of N_1 and N_{u2}.* They put

$$N_1 = \frac{\pi}{T_B/\lambda}, \quad N_{u2} = -\frac{2\pi U_\infty}{5\delta_+ u_\tau}. \quad \text{(A 5)}$$

They say 'experimental values of T_B/λ lie between 100 and 160, with 120 being a representative average for R_θ near 10^3', and accordingly we put

$$N_1 = \tfrac{1}{120}\pi, \quad \text{(A 6)}$$

although the frequency $N_1/2\pi = \frac{1}{240}$ seems to be rather small when compared with $\omega/2\pi = \frac{1}{100}$ in (2.5) and (2.7). As for N_{u2}, they cite $Re_\delta = 29000$, $\delta_+ = 1200$. Hence since $U_\infty/u_\tau = (\delta U_\infty/\nu)/(\delta u_\tau/\nu) = Re_\delta/\delta_+$, we are led to put

$$N_{u2} = \frac{2\pi}{5\delta_+}\frac{Re_\delta}{\delta_+} = \frac{2\pi}{5}\frac{20000}{(1200)^2}\left(\approx \frac{\pi}{124.1\ldots}\right). \quad \text{(A 7)}$$

However, if we adopt (A 6) and (A 7), the time period of (A 3) would be very long, and very long computational times would be required. We therefore assume simply

$$N_{u2} = \tfrac{1}{120}\pi = N_1, \quad \text{(A 8)}$$

recognizing that this may not agree with what CK have done.

(iii) *The values of ϕ_{u2} and ϕ_{w2}.* They reported that ϕ_{w2} has a major effect on the mean velocity profile of u, while ϕ_{u2} is not a sensitive parameter. Here we note that the importance of these parameters depends crucially on the ratio $\chi \equiv \frac{1}{2}N_{u2}/N_1$. It is not difficult to show that, in analysing quantities averaged over one time period, we may put without loss of generality

$$\phi'_{u2} \equiv \phi_{u2} - 2\pi(2\chi K + L), \quad \phi'_{w2} = \phi_{w2} - 2\pi(\chi K + M), \quad \text{(A 9)}$$

instead of ϕ_{u2}, ϕ_{w2} respectively in (A 3), where K, L and M are arbitrary integers. Unless χ is some special number, the distributions of Mod $(\phi'_{u2}, 2\pi)$ and Mod $(\phi'_{w2}, 2\pi)$ with $K = 0, \pm 1, \pm 2, \ldots$ are quite dense on $(0, 2\pi)$, and it would be difficult to find numerically a significant dependence of any quantity averaged over one period on ϕ_{u2} or ϕ_{w2}. (If χ is an irrational number, the flow cannot be periodic in time and ϕ_{u2}, ϕ_{w2} lose their meaning.) We have been unable to confirm CK's statement that ϕ_{w2} has a major effect on the mean velocity of u and assume here simply

$$\phi_{u2} = \phi_{w2} = 0. \tag{A 10}$$

CK represented the global pressure gradient associated with the large eddies as equivalent to the following body force:

$$F_1^+(t^+) = \frac{\partial u_{e2}^+}{\partial t^+}, \quad F_2^+ = 0, \quad F_3^+(t^+) = \frac{\partial w_{e2}^+}{\partial t^+}, \tag{A 11}$$

where $\boldsymbol{F}^+ = \boldsymbol{F}/(u_\tau^3/\nu)$, and u_{e2} and w_{e2} are the second terms of the right-hand sides of (A 3a) and (A 3c) respectively.

As for the initial velocity field, we put here

$$\boldsymbol{v} = 0 \quad (t = 0). \tag{A 12}$$

This is compatible with the treatment of CK, who used an 'arbitrary' initial condition.

Finally, to determine the velocity field uniquely under these boundary conditions, the uniform pressure gradient must be specified. We assume that it is zero,

$$\frac{1}{\lambda}\int_0^\lambda \frac{\mathrm{d}}{\mathrm{d}z} p(y, z)\,\mathrm{d}z = p(y, \lambda) - p(y, 0) = 0, \tag{A 13}$$

this being compatible with the assumption of constant stress in the wall layer.

To smooth the transition from the initial stage to the final periodic state, we introduced a damping factor for the boundary condition on $y = y_0$; i.e. instead of (A 3) we used

$$v^+(t^+) = \gamma(t^+) \times (\text{right-hand-side terms of (A 3)}) \quad (y = y_0^+), \tag{A 14}$$

where

$$\left.\begin{aligned} \gamma(t^+) &= 1 - \exp\left(\frac{-2t^+}{T_B}\right) \quad (t^+ < 2T_B), \\ &= 1 \qquad\qquad\quad (t^+ > 2T_B), \end{aligned}\right\} \tag{A 15}$$

$$T_B = \frac{\pi}{N_1} = 120.$$

We find that this improves the convergence to the final periodic state.

Appendix B. Suspected error in HH time advancement scheme

HH solved the vorticity equation (2.4) by the ADI method using an iterative procedure; the first iterate to ζ^{n+1}, say $\zeta^{n+1(1)}$, is obtained from ζ^n, ψ^n by solving

$$\frac{\zeta^{n+\frac{1}{2}} - \zeta^n}{\Delta t} = \ldots, \tag{B 1}$$

$$\frac{\zeta^{n+1} - \zeta^{n+\frac{1}{2}}}{\Delta t} = \ldots, \tag{B 2}$$

where ζ^n, ψ^n are the values of the nth time step. On the second iteration step (where they stopped), they substituted $\zeta^{n+1(1)}$ for ζ^n in the left-hand-side of (B 1). We think that this ζ^n should be left unchanged during the solution of (B 1), (B 2) which yields ζ^{n+1}. We tested their procedure by comparison with the well-known exact solution of (2.2)–(2.4):

$$\psi(y,z,t) = \exp\{-\nu(a^2+b^2)\,t\}\sin(ay)\sin(bz).$$

The numerical solution obtained in this way decayed nearly twice as fast as the exact one.

REFERENCES

ANTONOPOULOS-DOMIS, M. 1981 Aspects of large eddy simulation of homogeneous isotropic turbulence. *Int. J. Numer. Meth. in Fluids* **1**, 273.

CHAPMAN, D. R. & KUHN, G. D. 1981 Two-component Navier–Stokes computational model of viscous sublayer turbulence. *AIAA paper* **81**, 1024.

CLARK, R. A., FERZIGER, J. H. & REYNOLDS, W. C. 1979 Evaluation of subgrid-scale models using an accurately simulated turbulent flow. *J. Fluid Mech.* **91**, 1.

DEARDORFF, J. W. 1970 A numerical study of three-dimensional turbulent channel flow at large Reynolds numbers. *J. Fluid Mech.* **41**, 453.

FERZIGER, J. H. 1981 Higher-level simulations of turbulent flow. *Stanford University Rep.* TF-16.

HATZIAVRAMIDIS, D. T. & HANRATTY, T. J. 1979 The representation of the viscous wall region by a regular eddy pattern. *J. Fluid Mech.* **95**, 655.

JONES, W. P. & LAUNDER, B. E. 1973 The calculation of low-Reynolds-number phenomena with a two-equation model of turbulence. *Int. J. Heat Mass Transfer* **16**, 1119.

LAUFER, J. 1954 The structure of turbulence in fully developed pipe flow. *NACA Rep.* 1174.

LAUNDER, B. E. & SPALDING, D. B. 1972 *Mathematical Models of Turbulence*. Academic.

LEONARD, A. 1974 Energy cascade in large eddy simulation of turbulent fluid flows. *Adv. Geophys.* **18 A**, 237.

LESLIE, D. C. & QUARINI, G. L. 1979 The application of classical closures to the formulation of subgrid modelling procedures. *J. Fluid Mech.* **91**, 65.

LILLY, D. K. 1966 On the application of the eddy viscosity concept in the inertial subrange of turbulence. *NCAR Rep.* 123.

LILLY, D. K. 1967 The representation of small-scale turbulence in numerical simulation experiments. In *Proc. I.B.M. Scientific Computing Symp. on Environ. Sci.* 1966, p. 195.

MOIN, P. & KIM, J. 1982 Numerical investigation of turbulent channel flow. *J. Fluid Mech.* **118**, 341.

SCHUBERT, G. & CORCOS, G. H. 1967 The dynamics of turbulence near a wall according to a linear model. *J. Fluid Mech.* **29**, 113.

SCHUMANN, U. 1973 Ein Verfahren zur direkten numerischen simulation turbulenter Strömungen in Platten- und Ringspaltkanälen und über seine Anwendung zur Untersuchung von Turbulenzmodellen. Dissertation TH Karlsruhe, KFK 1854.

SCHUMANN, U. 1975 Subgrid scale model for finite difference simulations of turbulent flows in plane channels and annuli. *J. Comp. Phys.* **18**, 376.

SMAGORINSKI, J. 1963 General circulation experiments with the primitive equations. *Mon. Weather Rev.* **91**, 99.

ROBINSON, S. K. 1982 An experimental search for near-wall boundary conditions for large eddy simulation. In *Proc. AIAA/ASME 3rd Joint Thermodyn., Fluids, Plasma and Heat Transfer Conf.*